RNA (2002), *8*:913–923. Cambridge University Press. Printed in the USA.

DOI: 10.1017.S1355838202022057

Ribosomal proteins mediate the hepatitis C virus IRES–HeLa 40S interaction

GEOFF A. OTTO,[1,2] PETER J. LUKAVSKY,[1] ALISSA M. LANCASTER,[2] PETER SARNOW,[2] and JOSEPH D. PUGLISI[1]

[1]Department of Structural Biology, Stanford University School of Medicine, Stanford, California 94305-5126, USA
[2]Department of Microbiology and Immunology, Stanford University School of Medicine, Stanford, California 94305-5126, USA

ABSTRACT

Translation of the hepatitis C virus genomic RNA is mediated by an internal ribosome entry site (IRES). The 330-nt IRES RNA forms a binary complex with the small 40S ribosomal subunit as a first step in translation initiation. Here chemical probing and 4-thiouridine-mediated crosslinking are used to characterize the interaction of the HCV IRES with the HeLa 40S subunit. No IRES-18S rRNA contacts were detected, but several specific crosslinks to 40S ribosomal proteins were observed. The identity of the crosslinked proteins agrees well with available structural information and provides new insights into HCV IRES function. The protein-rich surface of the 40S subunit thus mediates the IRES–ribosome interaction.

Keywords: eukaryotic translation initiation protein–RNA complexes

INTRODUCTION

Translation initiation of the hepatitis C virus polyprotein is mediated by a structured RNA motif called an internal ribosome entry site (IRES; Tsukiyama-Kohara et al., 1992; Wang et al., 1993). The 330-nt HCV IRES is located in the 5′ untranslated region of the 9,500-nt HCV RNA genome. The HCV IRES has a highly conserved secondary structure based on phylogenetic and mutational analysis of HCV isolates and IRES motifs of closely related pestiviruses (Brown et al., 1992; Honda et al., 1999; Zhao & Wimmer, 2001). HCV IRES-regulated translation initiation occurs by a mechanism that is distinct from its eukaryotic host. Elucidation of the IRES mechanism will provide insight into an important part of the HCV replication cycle and eukaryotic translation in general.

In canonical eukaryotic translation initiation, a 5′ mRNA cap structure and a large multifactor protein complex (eIF4F) are required for the initial interaction between the mRNA and the small (40S) ribosomal subunit (reviewed in Sachs et al., 1997; Gingras et al., 1999). Subsequent to binding, correct positioning of the initiator AUG codon requires scanning of the 40S initiation complex towards the 3′ end of the mRNA (Kozak, 1986). In contrast, an uncapped HCV IRES RNA is capable of binding directly to a purified small (40S) ribosomal subunit in the absence of all additional protein factors. Upon binding to the 40S subunit, the IRES initiator AUG is directly positioned in, or near, the P-site (Pestova et al., 1998). The function of the IRES in this process is poorly understood.

A binary model system composed of the HCV IRES and 40S ribosomal subunit is a useful approximation for studying IRES function. With this model, 40S subunit contacts to the IRES have been determined (Kolupaeva et al., 2000; Lukavsky et al., 2000; Kieft et al., 2001) and guided structural (Klinck et al., 2000; Lukavsky et al., 2000) and mutational studies to examine their role in both IRES activity (Wang et al., 1993; Reynolds et al., 1995; Psaridi et al., 1999; Jubin et al., 2000) and 40S affinity (Kieft et al., 2001). These data reveal a lack of complete correlation between IRES binding affinity and activity. Therefore, during translation initiation, the HCV IRES likely has a more complicated regulatory function than simply binding to the small ribosomal subunit.

Uncovering these additional regulatory functions requires a better understanding of the nature of the interaction of the HCV IRES with the 40S subunit. A recent low-resolution cryo-EM structure of the HCV IRES–rabbit 40S subunit complex (Spahn et al., 2001) reveals the approximate location of the IRES on the outer surface of the 40S subunit, near the tRNA exit site

Reprint requests to: J.D. Puglisi, Department of Structural Biology, Stanford University School of Medicine, Stanford, California 94305-5126, USA; e-mail: puglisi@stanford.edu.

(E-site). From this study, it is not possible to identify whether the HCV IRES contacts 40S subunit ribosomal RNA or proteins. Here, chemical probing and 4-thiouridine-mediated crosslinking experiments were performed to determine the identity of these contact points. The HCV IRES forms specific, 4-thiouridine-dependent crosslinks with several different ribosomal proteins. The identity of these proteins provides new insights into IRES function.

RESULTS

Native gel analysis of the HCV IRES-HeLa 40S binary complex

Native gel analysis was performed to monitor the formation of the HCV IRES-HeLa 40S subunit binary complex under conditions similar to those employed in the crosslinking and chemical probing experiments. Under these conditions, the HCV IRES forms a specific, high affinity complex with HeLa 40S subunits. This complex should be representative of the interaction between the HCV IRES and hepatocellular 40S subunits, a more relevant biological target, as HeLa and hepatocellular ribosomes have similar protein composition (Schiffmann & Horak, 1978; Gressner, 1980). The mobility of the ^{32}P-5′-end-labeled HCV IRES shifts from the bottom of the gel in the free form to near the top of the gel upon the addition of excess HeLa 40S subunits (Fig. 1). No IRES mobility shift was observed for *Escherichia coli* 30S or HeLa 60S subunits (data not shown). In addition, no mobility shift was observed with *Saccharomyces cerevisiae* 40S (data not shown) in agreement with weak HCV IRES function in *S. cerevisiae* (P. Sarnow, unpubl. data). EDTA disrupts binary-complex formation, consistent with the expected stabilization of ribosomal subunits and IRES structure (Kieft et al., 1999) by Mg^{2+}. Partial protease treatment of the 40S subunit with either trypsin or proteinase K abrogates binary complex formation (data not shown). An affinity of 2 ± 1 nM for the HCV IRES-40S interaction was measured by competition with unlabeled wild-type IRES. This is identical to the value calculated by Kieft et al. (2001) using rabbit 40S subunits and filter binding.

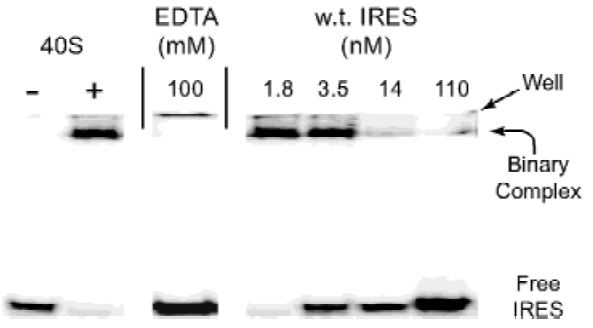

FIGURE 1. Autoradiograph of a 4% acrylamide native gel with 0.5 nM of ^{32}P-5′-end-labeled HCV IRES in the absence and presence of 5.5 nM purified HeLa 40S ribosomal subunits in the first and remaining lanes, respectively. The third lane included 100 mM EDTA during the incubation of IRES and 40S. The fourth through seventh lanes included increasing concentrations of unlabeled wild-type HCV IRES (from 1.8 to 110 nM) during the incubation.

Chemical probing of IRES-40S binary complex

Chemical probing is a useful tool to find potential interactions between solvent-accessible regions of RNA and external ligands. This technique was used to map possible contact points between the HCV IRES and HeLa 40S subunits. No IRES-dependent changes in RNA reactivity with DMS and kethoxal were observed in 18S rRNA (data not shown). The 40S subunits were saturated with IRES under the conditions of the probing experiments: A 10-fold excess of IRES over 40S was used at a concentration well above the K_d. Strong probing signals from other ribosome-ligand interactions, such as tRNA and 30S (Moazed & Noller, 1986), have been observed under similar reaction conditions. Although IRES-18S rRNA contacts may occur that are not observed by these chemical probing reagents, these data suggest that RNA–RNA contacts may not make a major contribution to the IRES-40S interaction.

Crosslinking the HCV IRES to 40S subunits with 4-thiouridine

4-thiouridine-mediated crosslinking was used to map further the interaction partners with the IRES on the 40S subunit. 4-thiouridine-mediated crosslinking is sensitive to intimate (<3 Å) interactions between a ligand and a single-stranded region of RNA (Dontsova et al., 1991; Wollenzien et al., 1991). Covalent crosslinks can occur to RNA or protein ligands by a free radical mechanism that is initiated by exposure to far UV (~365 nm) light. 4-thiouridine crosslinks are not detected from double-stranded regions of RNA, and, due to the small crosslink range, may be significantly altered by small conformational changes. In the IRES secondary structure, there are 66 uridines distributed in both single- and double-stranded regions (Fig. 2). Incorporation of multiple 4-thiouridines into the HCV IRES does not affect 40S binding affinity as measured by native mobility gel shift (data not shown), suggesting that the IRES structure is unaffected.

The HCV IRES forms specific, 4-thiouridine-dependent crosslinks to several different 40S ribosomal proteins, but not to 18S rRNA (data not shown). HCV IRES–40S binary complexes were formed under conditions similar to those used for native gel shifts with α-^{32}P body-labeled IRES and excess 40S subunits to facilitate protein staining. Binary complexes were irradiated at 365 nm on ice and then RNase

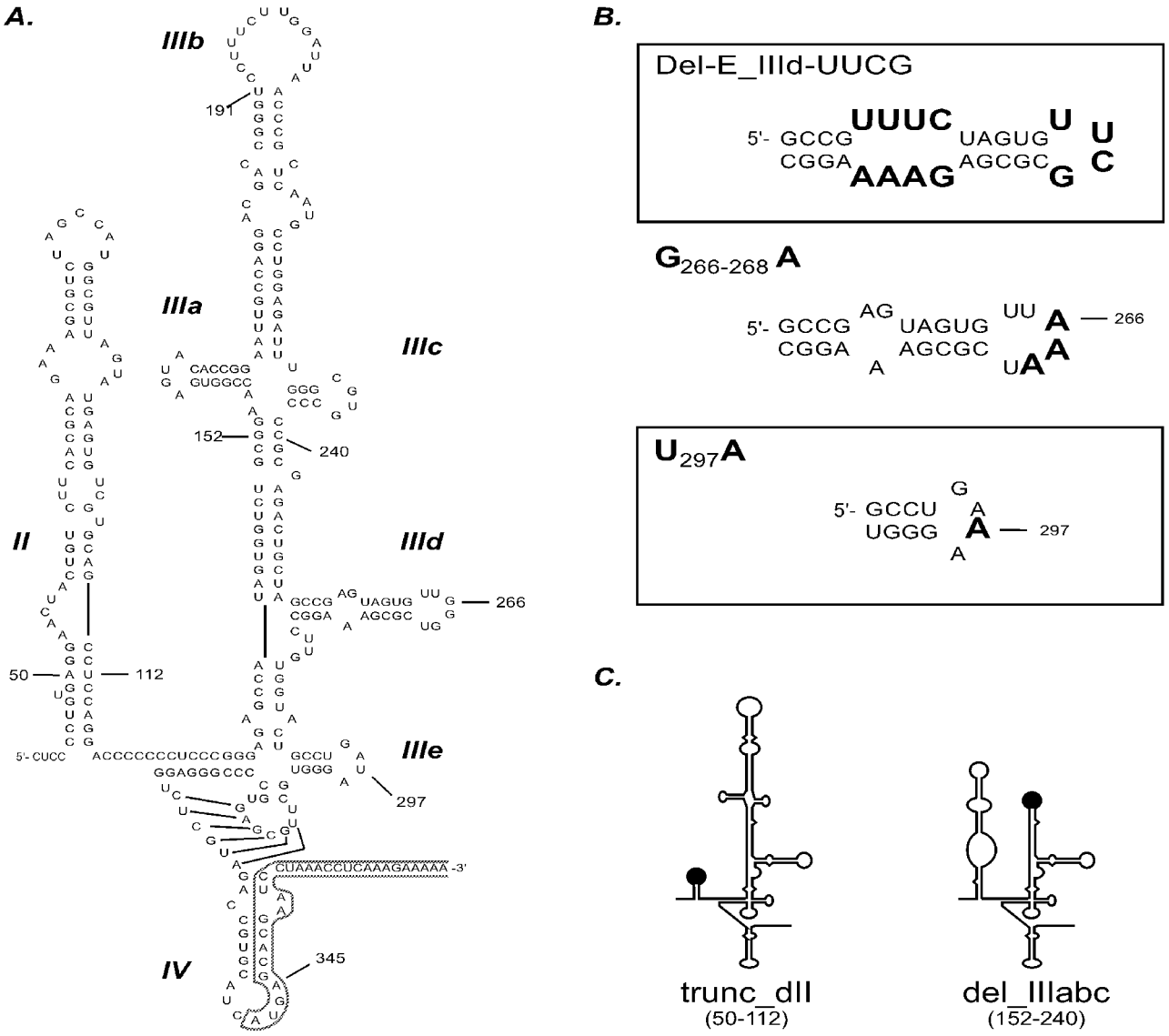

FIGURE 2. A: The HCV IRES secondary structure (Honda et al., 1999; Zhao and Wimmer, 2001; nt 40–370) is shown with the ORF boxed. **B:** The point mutants used in this study are illustrated with the mutated nucleotide(s) indicated in bold. **C:** Domain deletions are illustrated schematically. The deleted sequences, indicated by the black circle, were replaced with a UUCG tetraloop.

treated. Crosslinked proteins appear as radioactive bands from the covalently attached IRES fragment. Figure 3 shows a tris-tricine protein gel of a wild-type and mutant IRES crosslink reaction. Without 40S subunits or irradiation, no strong bands are observed (Fig. 3, lanes 1 and 2). The weak band present in Figure 3, lane 1 (RNA only control) is likely due to a residual interaction between the added RNase and labeled RNA oligonucleotides. Upon irradiation, several distinct strong bands are visible that are not observed without 4-thiouridine (data not shown). Crosslink band intensity is significantly reduced with the weakly binding ($K_d >$ 50 nM) triple mutant (delE_IIId-UUCG_U_{297}A) IRES (Fig. 3, lane 4). No crosslinks were observed to *Escherichia coli* 30S or HeLa 60S ribosomal proteins (data not shown), consistent with the low IRES affinity to these particles.

Two-dimensional gel electrophoresis is necessary to resolve the 31 ribosomal proteins of the 40S subunit

The first dimension of the gel separates proteins based on charge and the second on size. A silver-stained gel of 100 pmol of 40S subunits is shown in Figure 4. Assignment of the “core” 40S proteins was based upon comparison with prior work (Madjar et al., 1979), and MALDI-TOF analysis of excised bands performed here. In addition to the core ribosomal proteins, there are bands from several proteins that are tightly associated

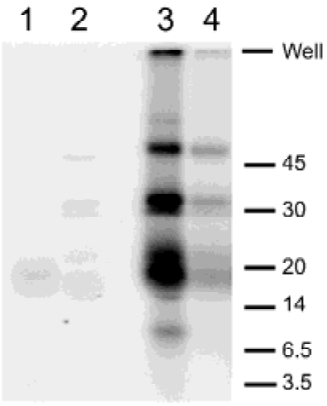

FIGURE 3. Autoradiograph of 4-thiouridine-mediated crosslink products between body-labeled HCV IRES and HeLa 40S subunits run on a tris-tricine protein gel. Lane 1 is an RNA-only control. Lanes 2 and 3 include wild-type HCV IRES and 40S subunits in the absence or presence of 365 nm irradiation, respectively. In lane 4, a mutant IRES, delE_IIId-UUCG_U_{297}A, with reduced 40S subunit affinity ($K_d >$ 50 nM) is crosslinked to 40S subunits. In lanes 2 to 4, ^{32}P body-labeled, 4-thiouridine IRES–40S binary complexes are formed under conditions used for native gels.

with the 40S subunit in unknown stoichiometry. Most of these proteins are consistently observed in different 40S preparations, resist dissociation with high salt (data not shown), and several have been observed in 40S subunits by other investigators (Madjar et al., 1979; Link et al., 1999). The identities of these additional proteins will be discussed below.

Two-dimensional gel analysis identifies HeLa 40S ribosomal proteins crosslinked to wild-type HCV IRES

The second dimension gel is silver stained and dried prior to autoradiography for assignment of the radioactive spots. The two-dimensional crosslinking pattern of wild-type IRES is shown in Figure 5 along with the corresponding overlay of ribosomal protein assignments. The crosslinking pattern and relative intensities are consistently observed in several independent experiments. The radioactive RNA oligonucleotide crosslinked to the protein causes a slight shift to the north (added mass) and west (increased negative charge) from the normal migration of the protein. Ribosomal proteins S2, S3, S10, S15, S27, and S16 or S18 form crosslinks with the HCV IRES. The crosslink to S2, as opposed to S3A, is resolved by running the first dimension at pH 7.2. At this pH, S3A moves a shorter distance, whereas the positions of S2 and the crosslink are unchanged (data not shown). Current and previous attempts to clearly resolve protein S16 from S18 have failed (Madjar et al., 1979). Similar migration of S16 and S18 under the different electrophoresis conditions tested is consistent with their similar size and charge distribution. The crosslinking pattern is unchanged upon addition of nt 1–43 (domain I) to the IRES construct (1–370) or the deletion of nt 345–370, which is the open reading frame (ORF) of the HCV polyprotein (data not shown). Thus the protein crosslinks occur to nt 44–344 of the IRES.

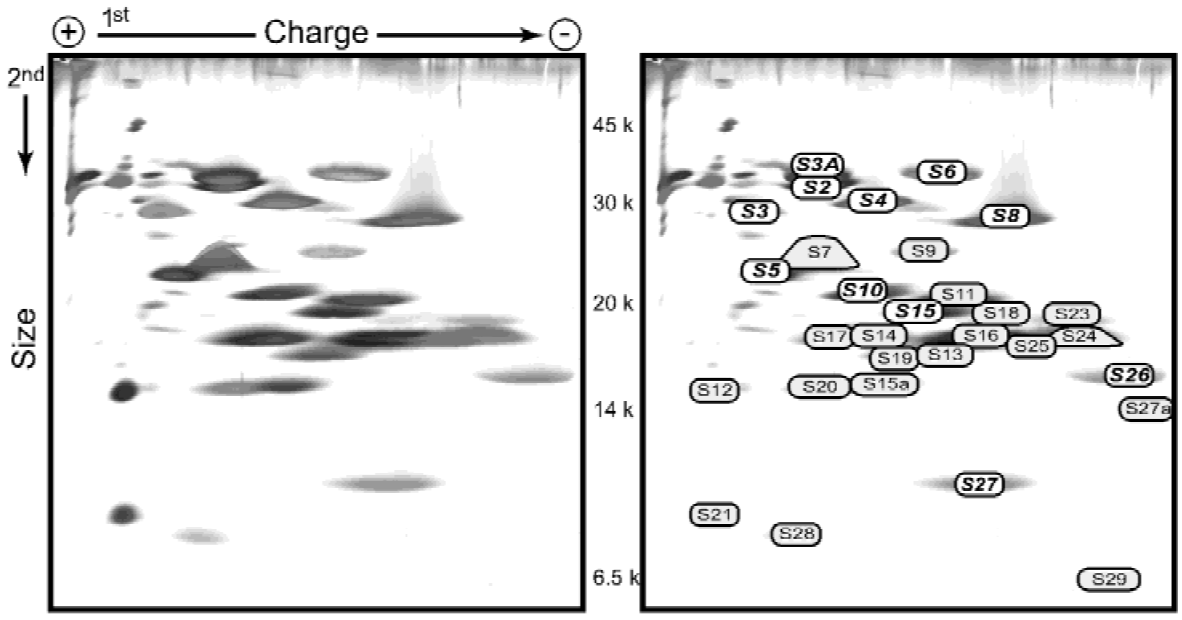

FIGURE 4. Two-dimensional gel analysis of proteins associated with the HeLa 40S ribosomal subunit. Proteins are separated based on charge at pH 5.5 in the first dimension and upon size in the second dimension. In the right panel, 40S core proteins are assigned by comparison to previous work (Madjar et al., 1979) indicated by lightly shaded boxes, and confirmed by MALDI-TOF analysis of excised bands (in bold italics).

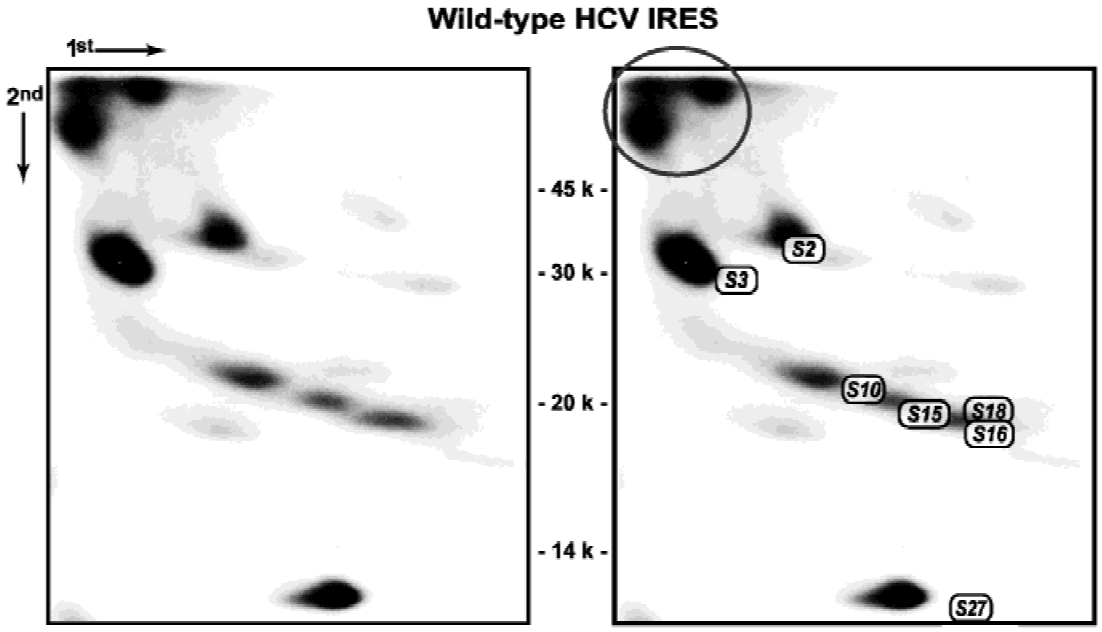

FIGURE 5. An autoradiograph of a two-dimensional gel containing HeLa 40S ribosomal proteins 4-thiouridine crosslinked to the wild-type HCV IRES. In the right panel, ribosomal protein spot assignments are superimposed on the autoradiogram based on silver staining. The circled radioactive bands in the upper left corner of the right panel could not be assigned by silver staining. Crosslinked proteins have a north-west shift from the added mass (north) and negative charge (west) of the crosslinked radioactive RNA oligonucleotide. Experiments were performed as in Figure 3.

The HCV IRES also forms crosslinks to two unknown proteins (upper left corner of Fig. 5) that are not core components of the 40S subunit. To increase the resolution of these bands, a lower acrylamide concentration was used for the second dimension, but even with extensive silver staining, a clear assignment of these spots was not possible. These crosslinks are lost in experiments performed with 40S subunits run through a poly(U)-Sepharose column (data not shown). In addition, the crosslinks are located north and west of spots observed when two-dimensional gels are western blotted with a polyclonal antibody raised against eIF3 (E. Jan, pers. comm.). These eIF3 spots are also lost in poly(U)-purified 40S subunits (data not shown). These observations suggest that the 40S subunits are contaminated with a small amount of eIF3, and offer circumstantial support that at least one of the unknown crosslinks is to a subunit of eIF3.

Mutant IRES constructs were tested to assign specific crosslinks, and potential functions, to different parts of the IRES

Several of the proteins crosslinked to wild-type IRES have prokaryotic homologs with known functions in translation (discussed below). Knowledge of which portions of the IRES interact with these proteins should provide more specific insights into IRES function. Because generating radioactive IRES constructs with site-specific incorporation of 4-thiouridine nucleotides is not feasible, IRES mutants were selected with the goal of disrupting a localized IRES–protein contact without significantly altering the global IRES-40S interaction. Maintenance of this global interaction is assumed to mirror IRES-40S affinity; so the four mutant constructs tested shown in Figure 2: $G_{266–268}A$ (~5 nM) and $U_{297}A$ (~1 nM) and trunc_dII (~6 nM) and del_IIIabc (~8 nM), all have near wild-type binding affinity. Relative to wild-type IRES, the four mutants evaluated consistently have similar relative percent distributions of crosslink intensities for proteins S2, S3, S15, and S16/S18, with S3 consistently the most intense (~35%) and S15 and S16/S18 the weakest (~8–10%). Both wild-type IRES and the trunc_dII mutant also share similar relative crosslink intensities for S10 and S27, ~10% and ~20%, respectively, despite the overall decrease in total crosslinking efficiency for trunc_dII (Fig. 6). The $G_{266–268}A$, $U_{297}A$, and del_IIIabc mutants all have greater crosslinking efficiency to S10 (~20%) than to S27 (~10%). All mutant constructs, except trunc_dII, showed similar crosslink intensities to the "unknown" proteins. The domain II truncation mutant showed significantly reduced crosslinking efficiency to the unknowns relative to wild type (compare circled regions in Figs. 5 and 6).

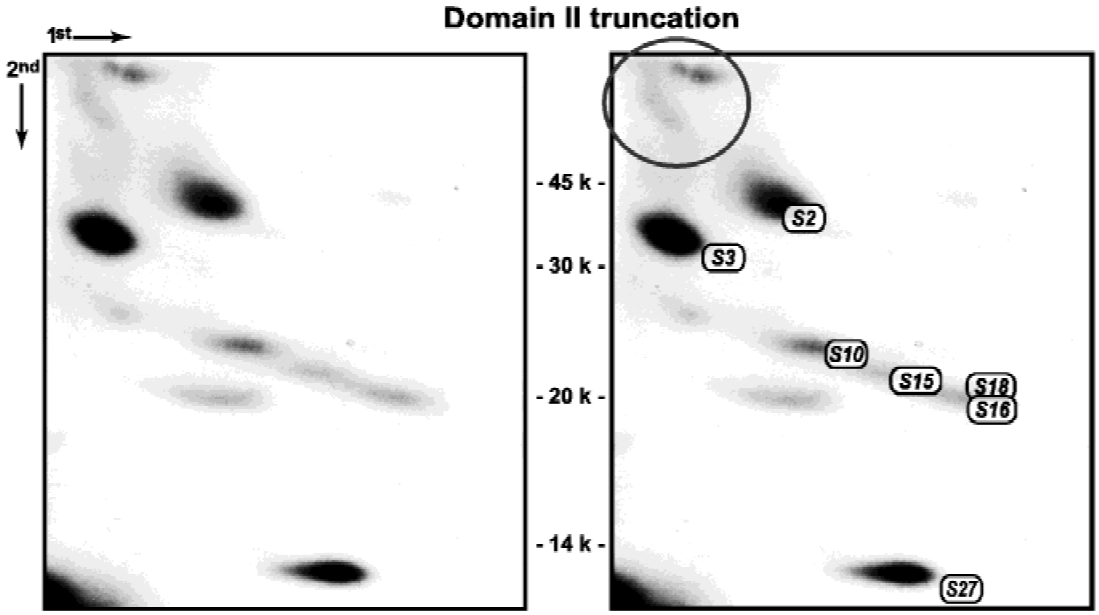

FIGURE 6. Autoradiograph showing a two-dimensional gel of the 4-thiouridine-mediated crosslinking between the domain II truncation IRES mutant and HeLa 40S subunits. The overall crosslinking intensity is proportionally reduced for all ribosomal proteins identified for wild type (Fig. 5), therefore preserving the relative crosslink intensities. The crosslinking to the unknowns, circle in upper left, is significantly reduced with the domain II truncation relative to wild type. Experiments were performed as in Figure 3.

DISCUSSION

Mapping contact points of the HCV IRES on HeLa 40S subunits

Defining areas of interaction between the HCV IRES and 40S subunits provides valuable insights into IRES mechanism. Earlier chemical and enzymatic probing experiments (Kolupaeva et al., 2000; Lukavsky et al., 2000; Kieft et al., 2001) have thoroughly mapped 40S contact points on the IRES. Recently, as the complexity of IRES function has become apparent, more attention has been focused on mapping IRES contacts on the 40S. The recent cryo-EM of the HCV IRES-40S complex provides the first picture of this interaction showing roughly where the IRES binds to the 40S (Spahn et al., 2001). A UV (254 nm) crosslinking study identified one protein, S5, that is likely to be important for this interaction (Fukushi et al., 2001).

To gain more information about the IRES-40S interaction, chemical probing and 4-thiouridine-mediated crosslinking were used. No contacts between IRES RNA and 18S rRNA were detected. No IRES-dependent changes in the DMS and Kethoxal chemical probing of 18S rRNA in the IRES-40S subunit binary complex were observed. Attempts to crosslink rRNA and the IRES also failed. These results are unexpected, as mRNAs docked into mRNA cleft of the small subunit have been footprinted on (Brow & Noller, 1983), and 4-thiouridine crosslinked to, rRNA (Graifer et al., 1994). The portion of the IRES ORF expected to associate with the mRNA binding cleft in the binary complex is predicted to form a stem-loop structure (domain IV), stabilization of which correlates with decreased IRES activity (Honda et al., 1996). This secondary structure could inhibit docking of the IRES into the mRNA cleft and prevent formation of the previously observed mRNA–rRNA interactions. Many RNA–RNA interactions, such as minor groove helix docking, are invisible to chemical probing and 4-thiouridine crosslinking, so IRES contact with 18S rRNA cannot be ruled out.

The HCV IRES forms specific crosslinks to 40S ribosomal proteins. Crosslinks to core 40S proteins were identified as S2, S3, S10, S15, S16 or S18, and S27. Proteins S2, S3, S15, and S16 or S18 are homologous to prokaryotic S5, S3, S19, and S9 or S13, respectively. S10 and S27 do not have prokaryotic homologs. Crosslinks to the two unknowns require domain II, and could be the result of a direct interaction with domain II or due to an induced conformational change in the IRES-40S binary complex. The failure to crosslink S5, homologous to prokaryotic S7, can be explained by the different interactions sampled by UV and 4-thiouridine-based crosslinking.

Structural context of IRES-40S protein crosslinks

The crosslinking data for the HCV IRES-HeLa 40S complex are in good agreement with available structural information. Cryo-EM reveals that the lower portion of

domain III binds to the solvent face of the Body of the 40S subunit on the E-site side, whereas the apical portion of domain III projects out into solution. Domain II hooks around the side of the Head and points down into the subunit interface. Comparison of the IRES-40S cryo-EM with crystal structures of the prokaryotic small (30S) ribosomal subunit (Schluenzen et al., 2000; Wimberly et al., 2000) provides a detailed context for this interaction and explains the observed crosslinks (Fig. 7). Proteins S2 and S3 are on the solvent face of the Body near domain III and S5, S15, and S16/S18 are E-site-side Head proteins located near domain II. The failure of the domain II truncation to abrogate crosslinking to proteins S15 and S16/S18 is not fully understood. These proteins could contact the basal portion of dII and their interactions would not be disrupted by the truncation. The crosslinks to these proteins could also be from interactions with other portions of the IRES (discussed below).

The HCV IRES thus binds to a protein-rich surface on the 40S subunit, consistent with the large number of interactions with ribosomal proteins, the lack of detectable interactions with 18S rRNA, and reduction in complex formation with protease treated 40S subunits. The binding site and proteins involved may also explain the inability of the HCV IRES to function in *S. cerevisiae* and bind to yeast 40S subunits. 18S rRNA is fairly similar between yeast and human (78% identity), whereas greater phylogenetic variation is observed for ribosomal protein sequences (average of 65% identity). Eukaryotic 40S subunits differ most in their protein components that make up the bulk of the solvent-accessible surface. Alignments of several *S. cerevisiae* and human ribosomal proteins identified to contact the IRES reveals large differences in S2, S5, and S10 (Fig. 8). Interactions with these proteins are probably important determinants of HCV IRES function.

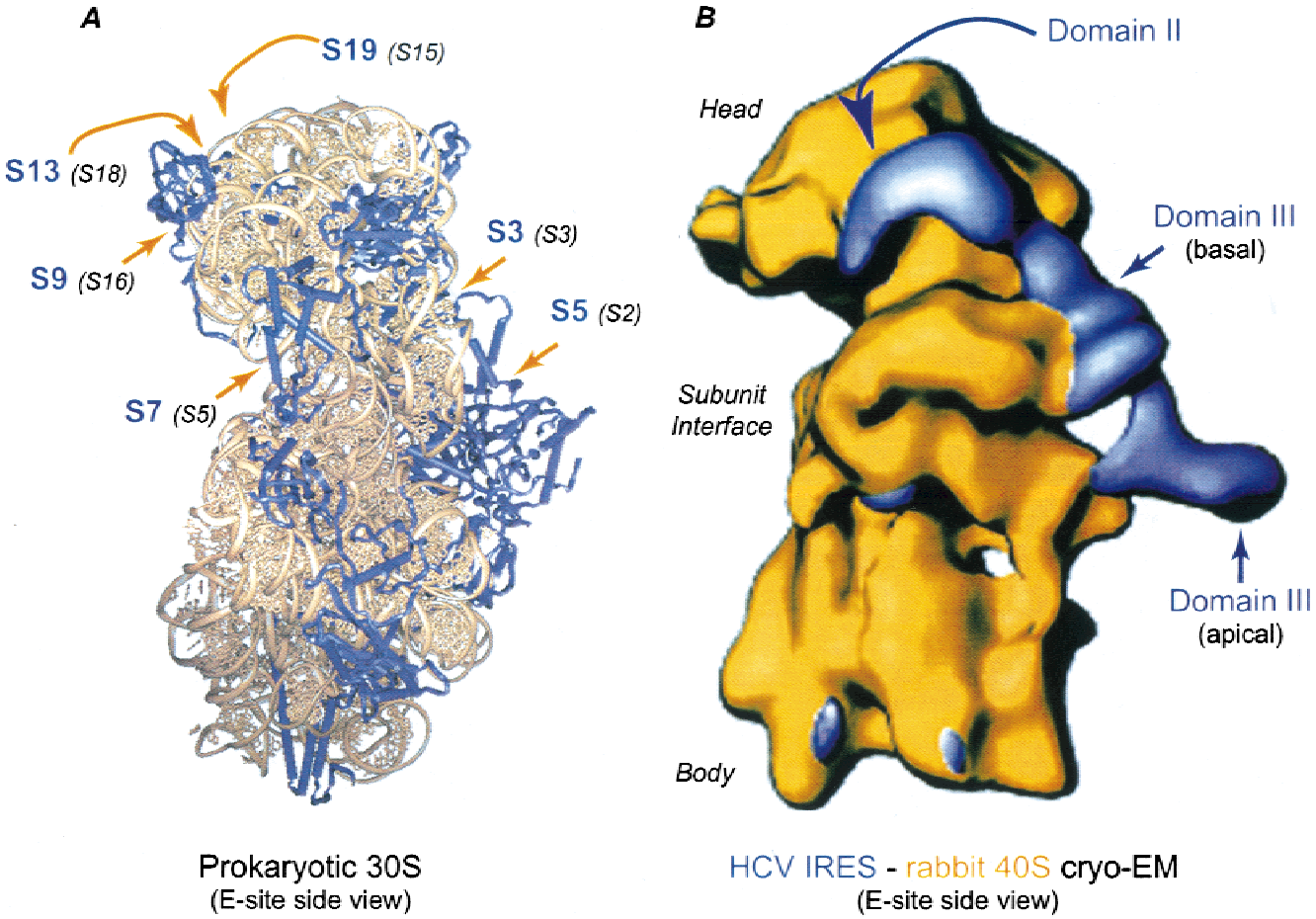

FIGURE 7. The E-site side views of prokaryotic 30S and HCV IRES–40S structures are shown. **A:** The high-resolution crystal structure of the *Thermus thermophilus* 30S subunit from Wimberly et al. (2000) adapted by Puglisi et al. (2000) with the 16S rRNA in tan and ribosomal proteins in blue. Locations of homologs of eukaryotic ribosomal proteins (in parentheses) that form 4-thiouridine crosslinks to the HCV IRES are indicated with arrows. **B:** The low-resolution cryo-EM of the HCV IRES–rabbit 40S subunit structure is adapted from Spahn et al. (2001) with the 40S subunit in orange and the IRES as the large blue structure.

FIGURE 8. The alignment of human and *S. cerevisiae* ribosomal protein S10 is shown. The protein sequences of human S10 (Accession: NM_001014) and *S. cerevisiae* S10 (Accession: NP_014936) are aligned with the ClustalW program (http://decypher.stanford.edu) and schematically presented with the Boxshade program. Identical residues are boxed in black (*) and similar residues are boxed in gray (.).

Novel contacts between domain II of the HCV IRES and eIF3 have been putatively identified and support the importance of modulating eIF3 activity for IRES function. Immuno-EM studies have localized eIF3, a large multisubunit complex, to the E-site face, spanning the Body and Head, of the 40S (summarized in Lutsch et al., 1990) directly adjacent to the HCV IRES binding site. This explains the domain IIIabc-eIF3 interaction (Sizova et al., 1998; Kieft et al., 2001) and accommodates our proposed interaction with domain II. During translation initiation, eIF3 modulates various aspects of 40S function—subunit association, ternary complex stabilization, and mRNA binding—in response to interactions with other components of the translation machinery (such as eIF4F; reviewed in Sonenberg et al., 2000). HCV IRES-mediated initiation does not require eIF4F, but requires regulatory events like those ascribed to eIF3. Contact between domains IIIabc and II and eIF3 could mediate IRES regulation of eIF3 function, thus partially explaining why these regions impact activity without affecting affinity.

Insights into HCV IRES mechanism

Coordinated regulation of 40S function by the HCV IRES is mediated through interactions with ribosomal proteins. Extrapolation from prokaryotic translation may explain how these interactions could modulate 40S function through IRES-dependent 40S conformational changes and more subtle effects. Changes in prokaryotic 30S function have been linked to observable conformational changes (Gabashvili et al., 1999; Frank & Agrawal, 2000) and to subtle alterations in ligand, for example, mRNA and tRNA, interactions (reviewed in Green & Noller, 1997). The HCV IRES interacts with two known Head proteins and induces a large conformational shift of the Head towards the Shoulder (on the A-site side) of the 40S. In the 30S subunit, a similar shift has been associated with mRNA binding and the translation initiation event. Part of the mRNA channel is formed by the noncovalent interaction of the Head and Shoulder of the 30S subunit (Gabashvili et al., 1999; Yusupova et al., 2001). Upon binding, prokaryotic initiation factor 1 causes movements of the Head towards the Shoulder of the 30S subunit (Carter et al., 2001).

The ribosomal proteins that interact with the HCV IRES are involved in mRNA and tRNA functions of the 40S subunit. Docking of the mRNA into the 40S subunit first requires formation of an IRES–40S complex. The primary 40S determinants of IRES affinity are still unknown. The crosslink to S3 is always the most intense and is not affected by either the truncation of domain II or the deletion of IIIabc, mutations that are known not to affect binding affinity (Kieft et al., 2001). The basal portion of domain III is the primary determinant of 40S binding affinity and is positioned immediately adjacent to S3. This suggests that S3 might be a major determinant of affinity in the IRES–40S complex, although the enhanced efficiency of crosslinking could also be a function of a more ideal juxtaposition of the 4-thiouridine and protein. After binding, the subsequent docking of the IRES ORF into the mRNA cleft requires the melting of domain IV stem-loop structure, in addition to 40S conformational changes. Domain IV melting could be regulated by the IRES interaction with S2 and S3; their 30S homologs have been implicated in mRNA helicase activity (Yusupova et al., 2001). The interaction with these two proteins could also shed light on the mechanism of HCV IRES release during initiation. 30S mRNA helicase activity is associated with Head-to-Body conformational changes that occur during translocation. Perhaps similar 40S conformational changes alter IRES binding and/or conformation and lead to IRES dissociation from the ribosome.

HCV IRES interactions with ribosomal proteins S2, S16/S18, and S5 could mediate regulation of 40S tRNA functions in the A-, P-, and E-sites, respectively. Proper IRES-mediated initiation probably requires efficient

recruitment of an aminoacyl tRNA to the A-site, establishment of the correct P-site codon–anticodon interaction, and proper positioning of the mRNA in the E-site. Prokaryotic S5 (S2 homolog) affects translational accuracy through effects on A-site tRNA affinity (Karimi & Ehrenberg, 1996). Increased A-site tRNA affinity has been observed from some S5 mutants. The conserved C-terminal tails of both S9 and S13 (homologs of S16 and S18, respectively) are involved in stabilizing the P-site codon–anticodon interaction (Yusupov et al., 2001). S7 (S5 homolog) binds to E-site tRNA and likely has a role in establishing the 5′ mRNA channel upstream of the AUG (Carter et al., 2000; Yusupov et al., 2001; Yusupova et al., 2001). All together, these data support the idea that the IRES is coordinately regulating 40S conformation and function of A-, P-, and E-site tRNAs and mRNA. The sensitivity of IRES activity to mutagenesis suggests that this coordinated regulation is essential for IRES function.

CONCLUSIONS

The IRES is a functionally dense RNA structure that regulates an essential step in the hepatitis C virus replication. An HCV IRES–40S binary complex model provides insight into IRES function during translation initiation. IRES function is mediated by an interaction with several 40S ribosomal proteins. These proteins could facilitate the coordinated regulation of A-, P-, and E-site tRNA–mRNA contacts, formation of the mRNA channel, 40S conformation, and initiation factor function. The relative importance of each of these potential contributions to IRES function is unknown and requires understanding interactions not present in the binary complex. A more complete understanding of HCV IRES function requires a more sophisticated model including initiation factors and tRNA.

MATERIALS AND METHODS

RNA preparation

Mutagenesis, expression, and purification of HCV IRES, strain 1b, were performed as described previously (Lukavsky et al., 2000). Constructs were cloned into pUC 119 for T7 run-off transcription. Small point mutations were made with the Quickchange Site Directed Mutagenesis kit (Pharmacia), large changes (domain deletions) were introduced by PCR. Deleted segments were replaced by a stable RNA tetraloop. In this study, wild-type IRES denotes the construct from nt 40 to 370 with the initiation AUG swapped for CUG to increase in vitro RNA stability (P. Lukavsky, unpubl. observation). For native gels, wild-type IRES RNA was end labeled by the exchange reaction and then purified. Transcriptions for crosslinking reactions included S_4UTP (Trilink Biotech), [α^{32}P] ATP, and [α^{32}P] CTP. Approximately 5 to 7 4-thiouridine nucleotides were incorporated per IRES.

HeLa S3 40S purification

Ribosomal subunits were purified as previously described (Lukavsky et al., 2000). HeLa S3 spinner cells were obtained from the National Cell Culture Center and gently lysed with Triton X-100. Lysates were spun briefly to remove debris and then layered onto a 30% (w/w) 0.5 M KCl sucrose cushion to pellet polysomes. Polysomes were resuspended, treated with puromycin (Blobel & Sabatini, 1971), returned to 0.5 M KCl and spun through a 10–30% sucrose gradient. The 40S and 60S peaks were detected at 260 nm, pooled, concentrated, and stored in 20 mM tris-HCL, pH 7.5, 0.2 mM EDTA, 150 mM KCl, 5 mM $MgCl_2$, 7% sucrose at −80 °C.

Native gel retardation

Conditions for native gel retardation have been previously described (Lorsch & Herschlag, 1999). 5′-end-labeled wild-type IRES (0.5 nM) was mixed with 5.5 nM purified 40S subunits in Buffer A (125 mM KOAc, 10 mM $MgCl_2$, 30 mM HEPES-KOH, pH 7.0, and 0.5 mM spermidine) plus 0.025% Triton X-100 to reduce aggregation. After incubation at 37 °C for 20 min, 50% sucrose was added, and the reactions were run on a 4% 37.5:1 acrylamide gel at 4 °C. For competition experiments, unlabeled IRES RNA was added in increments from 0.5 to 110 nM. Affinity measurements are based upon at least two independent repetitions. Gels were quantitated using a PhosphorImager.

Data was fit using Igor Pro (Wavemetrics). The following formula was used: fraction IRES bound $= (1/2T_t)\{K_T + (K_T/K_C)C_t + P_t + T_t - \sqrt{[K_T + (K_T/K_C)C_t + P_t + T_t]^2 - 4T_tP_t}\}$ (Long & Crothers, 1995), where C_t, P_t, and T_t, are the concentrations of 40S subunits, labeled wild-type IRES, and unlabeled competitor IRES, respectively (Long & Crothers, 1995). The dissociation constants for wild type–40S complexes and competitor–40S complexes are K_T and K_C, respectively. In agreement with Kieft et al. (2001), a single high affinity binding interaction between the IRES and 40S subunit was assumed and provided an excellent fit with the data.

Chemical probing

Kethoxal and DMS chemical probing of 18S rRNA was performed as described previously (Moazed et al., 1986; Lukavsky et al., 2000) under conditions similar to native gel analysis. Sites of base modification were detected by primer extension using 15 evenly spaced primers complimentary to different regions (Han et al., 1994). Body-labeled DNA products were resolved on an 8%, 7 M urea acrylamide gel and detected by autoradiography.

4-thiouridine-mediated crosslinking

4-thiouridine body-labeled IRES was mixed with an excess of 40S subunits in Buffer A, incubated at 37 °C and then placed on ice and immediately irradiated at 365 nm for 2 min with a handheld light source. Reactions were brought to 70 mM β-mercaptoethanol, 50 mM $MgCl_2$, 2 μg/mL RNase A, 100 U/mL RNase T_1, and incubated for 3 h at 37 °C. Proteins were extracted with 100 mM magnesium chloride in 67% acetic acid (Hardy et al., 1969) and acetone precipitated. For

one-dimensional tris-tricine gels (Schagger & von Jagow, 1987), the protein pellets were resuspended in tricine sample buffer (BioRad). For two-dimensional gel electrophoresis, the samples were resuspended in 10 M urea at 25 °C. The samples were then brought to 20 mM iodoacetamide for 30 min at 37 °C. Before loading, samples were spun through a P6 column (BioRad) equilibrated with 8 M urea, 40 mM bis-tris:HOAc, pH 4.2, 1% (v/v) βME. A 1:20 volume of 1 mg/mL of Basic Fuschin was added as a marker.

Two-dimensional gel electrophoresis

An acidic–tris-tricine gel system (Mets & Bogorad, 1974; Agafonov et al., 1999) is used in the BioRad Protean II. The first dimension tube gel (16 cm $\times$ 2 mm i.d.) was 4% acrylamide, 0.66% bis-acrylamide in 40 mM bis-tris:HOAc, pH 5.5. The gel was prerun in the same buffer for 4 h at 250 V maximum, 0.5 mA/tube with 10 mM L-cysteine methyl ester in the upper buffer well. For the run, the upper buffer well was 10 mM bis-tris:HOAc, pH 3.8, 1.7 mM 2-mercaptoethylamine and the bottom buffer was 10 mM bis-tris:HOAc, pH 6.0. The gel was run (1,000 V maximum, 0.25 mA/tube) for approximately 6 h, until the basic fuschin is $\sim$1 in. from the bottom of the tube. The tube gel was extruded onto a 16% acrylamide 0.6% bis-acrylamide tris-tricine gel with 8 M urea. A 6.4% stacking gel of 1 cm separated the tube gel from the separating. The second dimension was run for 6,000 V-h. The gel was silver or Coomassie stained and exposed to film (or PhosphorImager screen) to detect protein and crosslinked bands, respectively. Imagequant (Molecular Dynamics) was used to quantitate radioactive bands.

ACKNOWLEDGMENTS

We thank Scott Blanchard for invaluable assistance with two-dimensional gels, Eric Jan for useful discussions about 40S purification and eIF3 western blots, Jon Lorsch for help with the initial setup of the native gels, and Sunnie Thompson for assistance with *S. cerevisiae*. Dick Winant of the Stanford PAN facility performed the MALDI-TOF analysis of protein samples. This research was supported by National Institutes of Health (NIH) Grant A147365, an NIH training grant, the Hutchison Foundation, and Eli Lilly.

Received March 19, 2002; returned for revision
April 17, 2002; revised manuscript received May 6, 2002

REFERENCES

Agafonov DE, Kolb VA, Nazimov IV, Spirin AS. 1999. A protein residing at the subunit interface of the bacterial ribosome. *Proc Natl Acad Sci USA 96*:12345–12349.

Blobel G, Sabatini D. 1971. Dissociation of mammalian polyribosomes into subunits by puromycin. *Proc Natl Acad Sci USA 68*:390–394.

Brow DA, Noller HF. 1983. Protection of ribosomal RNA from kethoxal in polyribosomes. Implication of specific sites in ribosome function. *J Mol Biol 163*:27–46.

Brown EA, Zhang H, Ping LH, Lemon SM. 1992. Secondary structure of the 5′ nontranslated regions of hepatitis C virus and pestivirus genomic RNAs. *Nucleic Acids Res 20*:5041–5045.

Carter AP, Clemons WM Jr, Brodersen DE, Morgan-Warren RJ, Hartsch T, Wimberly BT, Ramakrishnan V. 2001. Crystal structure of an initiation factor bound to the 30S ribosomal subunit. *Science 291*:498–501.

Carter AP, Clemons WM, Brodersen DE, Morgan-Warren RJ, Wimberly BT, Ramakrishnan V. 2000. Functional insights from the structure of the 30S ribosomal subunit and its interactions with antibiotics. *Nature 407*:340–348.

Dontsova O, Kopylov A, Brimacombe R. 1991. The location of mRNA in the ribosomal 30S initiation complex; site-directed cross-linking of mRNA analogues carrying several photo-reactive labels simultaneously on either side of the AUG start codon. *EMBO J 10*: 613–620.

Frank J, Agrawal RK. 2000. A ratchet-like inter-subunit reorganization of the ribosome during translocation. *Nature 406*:318–322.

Fukushi S, Okada M, Stahl J, Kageyama T, Hoshino FB, Katayama K. 2001. Ribosomal protein S5 interacts with the internal ribosomal entry site of hepatitis C virus. *J Biol Chem 276*:20824–20826.

Gabashvili IS, Agrawal RK, Grassucci R, Squires CL, Dahlberg AE, Frank J. 1999. Major rearrangements in the 70S ribosomal 3D structure caused by a conformational switch in 16S ribosomal RNA. *EMBO J 18*:6501–6507.

Gingras AC, Raught B, Sonenberg N. 1999. eIF4 initiation factors: Effectors of mRNA recruitment to ribosomes and regulators of translation. *Annu Rev Biochem 68*:913–963.

Graifer DM, Juzumiene DI, Wollenzien P, Karpova GG. 1994. Crosslinking of mRNA analogues containing 4-thiouridine residues on the 3′- or 5′-side of the coding triplet to the mRNA binding center of the human ribosome. *Biochemistry 33*:3878–3884.

Green R, Noller HF. 1997. Ribosomes and translation. *Annu Rev Biochem 66*:679–716.

Gressner AM. 1980. Human liver ribosomal proteins: Characterization by two-dimensional electrophoresis and molecular weight determinations. *Biochem Med 23*:350–357.

Han H, Schepartz A, Pellegrini M, Dervan PB. 1994. Mapping RNA regions in eukaryotic ribosomes that are accessible to methidiumpropyl-EDTA.Fe(II) and EDTA.Fe(II). *Biochemistry 33*: 9831–9844.

Hardy SJ, Kurland CG, Voynow P, Mora G. 1969. The ribosomal proteins of *Escherichia coli*. I. Purification of the 30S ribosomal proteins. *Biochemistry 8*:2897–2905.

Honda M, Beard MR, Ping LH, Lemon SM. 1999. A phylogenetically conserved stem-loop structure at the 5′ border of the internal ribosome entry site of hepatitis C virus is required for cap-independent viral translation. *J Virol 73*:1165–1174.

Honda M, Brown EA, Lemon SM. 1996. Stability of a stem-loop involving the initiator AUG controls the efficiency of internal initiation of translation on hepatitis C virus RNA. *RNA 2*:955–968.

Jubin R, Vantuno NE, Kieft JS, Murray MG, Doudna JA, Lau JY, Baroudy BM. 2000. Hepatitis C virus internal ribosome entry site (IRES) stem loop IIId contains a phylogenetically conserved GGG triplet essential for translation and IRES folding. *J Virol 74*:10430–10437.

Karimi R, Ehrenberg M. 1996. Dissociation rates of peptidyl-tRNA from the P-site of *E. coli* ribosomes. *EMBO J 15*:1149–1154.

Kieft JS, Zhou K, Jubin R, Doudna JA. 2001. Mechanism of ribosome recruitment by hepatitis C IRES RNA. *RNA 7*:194–206.

Kieft JS, Zhou K, Jubin R, Murray MG, Lau JY, Doudna JA. 1999. The hepatitis C virus internal ribosome entry site adopts an ion-dependent tertiary fold. *J Mol Biol 292*:513–529.

Klinck R, Westhof E, Walker S, Afshar M, Collier A, Aboul-Ela F. 2000. A potential RNA drug target in the hepatitis C virus internal ribosomal entry site. *RNA 6*:1423–1431.

Kolupaeva VG, Pestova TV, Hellen CU. 2000. An enzymatic footprinting analysis of the interaction of 40S ribosomal subunits with the internal ribosomal entry site of hepatitis C virus. *J Virol 74*:6242–6250.

Kozak M. 1986. Point mutations define a sequence flanking the AUG initiator codon that modulates translation by eukaryotic ribosomes. *Cell 44*:283–292.

Link AJ, Eng J, Schieltz DM, Carmack E, Mize GJ, Morris DR, Garvik BM, Yates JR III. 1999. Direct analysis of protein complexes using mass spectrometry. *Nat Biotechnol 17*:676–682.

Long KS, Crothers DM. 1995. Interaction of human immunodeficiency virus type 1 Tat-derived peptides with TAR RNA. *Biochemistry 34*:8885–8895.

Lorsch JR, Herschlag D. 1999. Kinetic dissection of fundamental processes of eukaryotic translation initiation in vitro. *EMBO J 18*:6705–6717.

Lukavsky PJ, Otto GA, Lancaster AM, Sarnow P, Puglisi JD. 2000. Structures of two RNA domains essential for hepatitis C virus internal ribosome entry site function. *Nat Struct Biol 7*:1105–1110.

Lutsch G, Stahl J, Kargel HJ, Noll F, Bielka H. 1990. Immunoelectron microscopic studies on the location of ribosomal proteins on the surface of the 40S ribosomal subunit from rat liver. *Eur J Cell Biol 51*:140–150.

Madjar JJ, Arpin M, Buisson M, Reboud JP. 1979. Spot position of rat liver ribosomal proteins by four different two-dimensional electrophoreses in polyacrylamide gel. *Mol Gen Genet 171*:121–134.

Mets LJ, Bogorad L. 1974. Two-dimensional polyacrylamide gel electrophoresis: An improved method for ribosomal proteins. *Anal Biochem 57*:200–210.

Moazed D, Noller HF. 1986. Transfer RNA shields specific nucleotides in 16S ribosomal RNA from attack by chemical probes. *Cell 47*:985–994.

Moazed D, Stern S, Noller HF. 1986. Rapid chemical probing of conformation in 16 S ribosomal RNA and 30 S ribosomal subunits using primer extension. *J Mol Biol 187*:399–416.

Pestova TV, Shatsky IN, Fletcher SP, Jackson RJ, Hellen CU. 1998. A prokaryotic-like mode of cytoplasmic eukaryotic ribosome binding to the initiation codon during internal translation initiation of hepatitis C and classical swine fever virus RNAs. *Genes & Dev 12*:67–83.

Psaridi L, Georgopoulou U, Varaklioti A, Mavromara P. 1999. Mutational analysis of a conserved tetraloop in the 5′ untranslated region of hepatitis C virus identifies a novel RNA element essential for the internal ribosome entry site function. *FEBS Lett 453*: 49–53.

Puglisi JD, Blanchard SC, Green R. 2000. Approaching translation at atomic resolution. *Nat Struct Biol 7*:855–861.

Reynolds JE, Kaminski A, Kettinen HJ, Grace K, Clarke BE, Carroll AR, Rowlands DJ, Jackson RJ. 1995. Unique features of internal initiation of hepatitis C virus RNA translation. *EMBO J 14*:6010–6020.

Sachs AB, Sarnow P, Hentze MW. 1997. Starting at the beginning, middle, and end: Translation initiation in eukaryotes. *Cell 89*:831–838.

Schagger H, von Jagow G. 1987. Tricine-sodium dodecyl sulfate-polyacrylamide gel electrophoresis for the separation of proteins in the range from 1 to 100 kDa. *Anal Biochem 166*:368–379.

Schiffmann D, Horak I. 1978. Ribosomal proteins of HeLa cells. *Eur J Biochem 82*:91–95.

Schluenzen F, Tocilj A, Zarivach R, Harms J, Gluehmann M, Janell D, Bashan A, Bartels H, Agmon I, Franceschi F, Yonath A. 2000. Structure of functionally activated small ribosomal subunit at 3.3 Angstroms resolution. *Cell 102*:615–623.

Sizova DV, Kolupaeva VG, Pestova TV, Shatsky IN, Hellen CU. 1998. Specific interaction of eukaryotic translation initiation factor 3 with the 5′ nontranslated regions of hepatitis C virus and classical swine fever virus RNAs. *J Virol 72*:4775–4782.

Sonenberg N, Hershey JWB, Mathews M. 2000. *Translational control of gene expression*, 2nd ed. Cold Spring Harbor, New York: Cold Spring Harbor Laboratory Press.

Spahn CM, Kieft JS, Grassucci RA, Penczek PA, Zhou K, Doudna JA, Frank J. 2001. Hepatitis C virus IRES RNA-induced changes in the conformation of the 40s ribosomal subunit. *Science 291*: 1959–1962.

Tsukiyama-Kohara K, Iizuka N, Kohara M, Nomoto A. 1992. Internal ribosome entry site within hepatitis C virus RNA. *J Virol 66*:1476–1483.

Wang C, Sarnow P, Siddiqui A. 1993. Translation of human hepatitis C virus RNA in cultured cells is mediated by an internal ribosome-binding mechanism. *J Virol 67*:3338–3344.

Wimberly BT, Brodersen DE, Clemons WM Jr, Morgan-Warren RJ, Carter AP, Vonrhein C, Hartsch T, Ramakrishnan V. 2000. Structure of the 30S ribosomal subunit. *Nature 407*:327–339.

Wollenzien P, Expert-Bezancon A, Favre A. 1991. Sites of contact of mRNA with 16S rRNA and 23S rRNA in the *Escherichia coli* ribosome. *Biochemistry 30*:1788–1795.

Yusupov MM, Yusupova GZ, Baucom A, Lieberman K, Earnest TN, Cate JH, Noller HF. 2001. Crystal structure of the ribosome at 5.5 Å resolution. *Science 292*:883–896.

Yusupova GZ, Yusupov MM, Cate JH, Noller HF. 2001. The path of messenger RNA through the ribosome. *Cell 106*:233–241.

Zhao WD, Wimmer E. 2001. Genetic analysis of a poliovirus/hepatitis C virus chimera: New structure for domain II of the internal ribosomal entry site of hepatitis C virus. *J Virol 75*:3719–3730.